Numer. Math. Theor. Meth. Appl.
doi: 10.4208/nmtma.2015.w02si

Vol. **8**, No. 1, pp. 97-111
February 2015

A Multilevel Method for the Solution of Time Dependent Optimal Transport

Eldad Haber* and Raya Horesh

Department of Mathematics & Department of Earth and Ocean Science, The University of British Columbia, Vancouver, BC, Canada; IBM research, NY, USA.

Received 30 October 2013; Accepted 22 June 2014

Abstract. In this paper we present a new computationally efficient numerical scheme for the minimizing flow for the computation of the optimal L_2 mass transport mapping using the fluid approach. We review the method and discuss its numerical properties. We then derive a new scaleable, efficient discretization and a solution technique for the problem and show that the problem is equivalent to a mixed form formulation of a nonlinear fluid flow in porous media. We demonstrate the effectiveness of our approach using a number of numerical experiments.

AMS subject classifications: 15A12, 65F10, 65F15

Key words: Optimal mass transport, inverse problems, staggered grids.

1. Introduction

Optimal mass transport is of cardinal importance in geoscience and engineering with other applications in econometrics, fluid dynamics, automatic control, transportation, statistical physics, shape optimization, expert systems, and meteorology [26, 31]. The problem was first formulated by the civil engineer Gaspar Monge in 1781, and concerns with finding an optimal way, in the sense of minimal transportation cost, of moving a pile of soil from one site to another. Much later the problem was extensively analyzed by Kantorovich [21], and is now known as the Monge-Kantorovich problem.

There are several formulations of the problem [2, 26, 31] of varying degrees of generality. Here we start with the formulation of the Monge-Kantorovich problem for smooth densities and domains in Euclidean space (for more general measures, see [2]). Let Ω_0 and Ω_1 be two diffeomorphic connected subdomains of $\mathbb{R}^d$, and let μ_0, μ_1 be

*Corresponding author. *Email address:* haber@math.ubc.ca (E. Haber)

 ©2015 Global-Science Press

https://doi.org/10.4208/nmtma.2015.w02si Published online by Cambridge University Press

Borel measures on Ω_0 and Ω_1, each with a strictly positive density function $\mu_0(x) \geq \mu_{\text{low}}^0 > 0$ and $\mu_1 \geq \mu_{\text{low}}^1 > 0$, respectively. Assume

$$\int_{\Omega_0} \mu_0(x)dx = \int_{\Omega_1} \mu_1(x)dx,$$

so that the same total mass is associated with Ω_0 and Ω_1.

Under some mild assumptions, the Monge-Kantorovich problem may be expressed as the following optimization problem

$$\min \quad M(u) := \frac{1}{p}\int_{\Omega} \mu_0(x)|u(x)|^p \, dx \tag{1.1a}$$

$$\text{s.t.} \quad c(u) = \det(I_d + \nabla u)\mu_1(x + u(x)) - \mu_0(x) = 0, \tag{1.1b}$$

where u is a $C^{1,\alpha}$ diffeomorphism from $\Omega_0 \to \Omega_1$. The constraint $c(u) = 0$ (the Jacobian equation) is often referred to as the mass preserving (MP) property. Here, we consider the classical case of $p = 2$ as well as $1 < p \leq 2$ and attempt to numerically address the limiting (ill-posed) case when $p = 1$.

Even with a simple, quadratic distance function, the problem (1.1) is regarded as a highly nonlinear equality constrained optimization problem. Extensive analysis as for the existence, uniqueness, and properties of the solution is available (see for example [2, 15, 31] and the references therein). However, while a large body of literature deals with the analysis of the problem, surprisingly a relatively small number of papers concern with finding numerical solutions to the problem, and even a smaller number of publications that deal with devising *efficient*, that is, scalable, numerical solutions for this challenging problem [3, 5, 11–13, 19, 24].

Generally speaking, numerical methods for the solution of the problem can be divided into three approaches. In the first approach, for the case $p = 2$, one utilizes the property that $u = \nabla\phi$ where ϕ is a concave function and solves the Monge-Ampère equation [14, 25]. The second approach attempts to tackle the constrained optimization problem head-on. Among this work is our previous algorithm [19].

A third approach for the solution of the problem, which is the starting point of this study was proposed in the seminal paper of Benamou and Brenier [5]. Their research reconstructs an optimal path from μ_0 to μ_1 by solving a convex optimization problem with a linear space-time transport partial differential equation as a constraint. Their approach is particularly useful if the transportation path is needed. Its disadvantage is that it increases the dimensionality of the problem by recasting the problem as a space-time control problem. In the original work of Benamou and Brenier, simple nodal discretization was used, combined with the augmented Lagrangian method for the solution of the problem. When reproducing the results of the paper we have observed some stability issues as well as deterioration of the algorithm for large-scale problems. As we show in this work this instability can be explained by analyzing their discretization using multigrid tools (Fourier analysis) that show that the discretization is not h-elliptic.

https://doi.org/10.4208/nmtma.2015.w02si Published online by Cambridge University Press

Nonetheless, the Benamou and Brenier method replaces a generally non-convex problem with a convex one and further avoids some other intricacies such as boundary conditions and difficulties when the density contrasts are large. In fact, for the latter case all algorithms known to us have failed when the density contrast between μ_0 and μ_1 was larger than 50.

Given the lack of efficient *numerical techniques* for the solution of the problem, the goal of this study is to develop a numerical solution framework, based upon the Benamou-Brenier fluid dynamics formulation. We require this algorithm to be stable fast and efficient (with linear complexity), capable of resolving problems comprising large density contrast, and lastly, we aim at design of generic formulation, for which alternative cost functionals can be readily incorporated, such as [27]. We point that non of the algorithms in use today can claim linear complexity for the problem.

The paper is structured as follows. In Section 2 we reformulate the problem by following the Benamou and Brenier derivation and present its extension to more general L_p functionals. In Section 3 we introduce a conservative discretization of the problem. In Section 4 we describe the optimization algorithm and the linear solver used to solve the optimization problem and the linear systems that arise in the solution process. In Section 5 we conduct few numerical experiments and finally, in Section 6 we summarize the paper.

2. Problem reformulation

Let us consider the time interval $t \in [0,1]$. The idea of Benamou-Brenier was to replace the non-convex problem (1.1) with an optimization problem, constrained by a partial differential equation

$$\min \quad \int_{t=0}^{1} \int_{\Omega} \rho(x,t)|v(x,t)|^2 \, dx \, dt \tag{2.1a}$$

$$\text{s.t.} \quad \frac{\partial \rho}{\partial t} + \nabla \cdot (\rho v) = 0, \tag{2.1b}$$

$$\rho(x,0) = \mu_0, \quad \rho(x,1) = \mu_1. \tag{2.1c}$$

Here, $v(x,t)$ is the velocity and $\rho(x,t) > 0$ is the density. This formulation essentially describes the evolution of the mass density distribution ρ_0 to the distribution ρ_1, where minimal energy is invested, while the mass obeys a mass-preserving PDE. The above problem falls into the PDE constrained optimization problems category. Generic solutions for this family of problems were recently presented in the literature (see for example, [7,8,17] and reference within). In the context of PDE optimization problems the density, ρ, is the state and the velocity, v, is the control. One then minimizes the objective function subject to fulfilment of the PDE constraints. This formulation is similar to the one solved in [8].

While conventional PDE optimization methods can be used here, there are some obvious limitations to their use. The main limitation is related to the underlying assumption that given the controls, v, the PDE can be solved independently from the

https://doi.org/10.4208/nmtma.2015.w02si Published online by Cambridge University Press

optimization problem. For the problem (2.1) this is not the case. Note that there are no boundary conditions (BC) for ρ in the PDE and thus one cannot solve for ρ even if v is known without introducing (unnecessary) boundary conditions. Although it is possible to "fake" boundary conditions (and this has been done), such boundary conditions can bring disastrous effects upon the reconstruction. For example, the use of some inflow and outflow BC strongly biases v, similarly, periodic BC (used in the original work of [5]) are non-physical. As we see next, BC for ρ are actually not needed in order to solve the problem. In fact, resolving the boundary conditions is an integral part of the optimization problem. To see that, we continue and follow Benamou-Brenier formulation by setting the momentum $m = \rho v$ and replacing (2.1) with a convex optimization problem

$$\min \quad f(m,\rho) = \int_{t=0}^{1}\int_{\Omega} \frac{|m(x,t)|^2}{\rho(x,t)}\,dx\,dt \tag{2.2a}$$

$$\text{s.t.} \quad c(m,\rho) = \rho_t + \nabla\cdot\, m = 0, \tag{2.2b}$$

$$\rho(x,0) = \mu_0, \quad \rho(x,1) = \mu_1. \tag{2.2c}$$

It is interesting to note that the above problem has the same structure as of mixed form of non-linear flow in porous media [23]. This become apparent by setting $w = (m,\rho)^\top = (m_1,\cdots,m_d,\rho)^\top$, where d is the dimension of the problem, and rewriting the problem as

$$\begin{aligned} \min \quad & f(w) \\ \text{s.t.} \quad & \nabla^{\text{st}}\cdot\, w = 0, \end{aligned}$$

where $\nabla^{\text{st}}\cdot$ is the space-time divergence. If we treat time as a spatial dimension then the MK problem and non-linear flow in porous media have the exact same general variational form (see [4, 9, 23]). Furthermore, it is well-known that such problems are well-posed as long as f is smooth and convex even in the absence of boundary conditions for $w_{d+1} = \rho$. As we shall see later, similar to other mixed form of elliptic problems [9], the lack of BC for ρ leads to BC for the Lagrange multipliers. To illustrate this notion over the simplest case, let

$$f(w) = \int_{\Omega} |w|^2\,dx.$$

For this objective, a classical result yields the mixed form of the Poisson equation [9]. Thus, we see that the optimization problem at hand is nothing but a nonlinear Poisson-like equation that regularly solved for ground water flow [4, 22].

This similarity to the mixed form of flow in porous media in mixed form, motivates our research here. A large body of literature and highly efficient algorithms have been developed for such problems (e.g. [20, 22] and many others). It is merely sensible on our behalf to put this techniques into good use. Understanding this similarity also helps in developing robust and stable discretization, choosing efficient optimization

https://doi.org/10.4208/nmtma.2015.w02si Published online by Cambridge University Press

algorithms and indicate efficient solvers for the linear systems. We address each of these components separately in the following sections.

The above consideration allows us to easily consider alternative convex functionals. For example, we may consider the function $|v|^p\rho(x)$, which lend itself to the energy

$$\frac{|v(x,t)|^p}{\rho(x,t)} = \frac{|m(x,t)|^p}{\rho(x,t)^{p-1}}. \tag{2.3}$$

This functional is strictly convex for $1 < p \leq 2$. Interestingly, for the case $p = 1$ we obtain that the energy is reduced to $|m|$ that is non-differentiable. Nonetheless, in our numerical test we consider a sequence of p's that converges to $p = 1$ as a possible approach in computing the L_1 solution.

3. Discretization

It is important to note that discretization of optimization problems consisting of differential constraints may not be straightforward. In fact, instabilities may arise if naïve discretization techniques are used. This topic has been studied extensively for the Stokes problem and for flow in porous media (see for example [9, 30] and reference within). To obtain stable discretizations using finite difference or finite volume, h-ellipticity criterion needs to be met. For finite element discretization the Ladysenskaja, Babuska, Brezzi (LBB) conditions need to be fulfilled [9]. Thus, special attention must be given to maintain stability in such problems.

Here we propose to use a finite volume approach in space-time. For simplicity of the discussion we describe the discretization in 2D and time. The extension to 3D is straightforward and will be experimented with in Section 5.

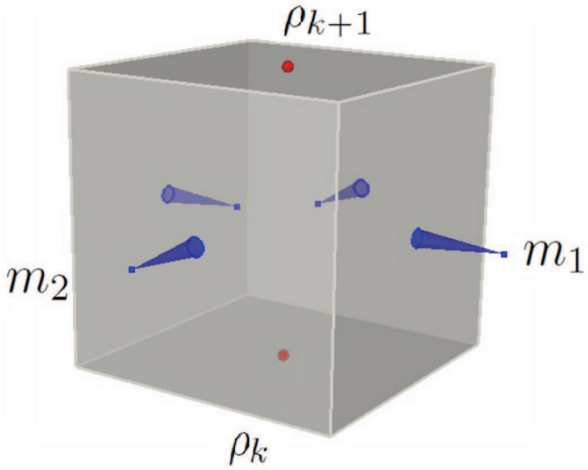


Figure 1: A box and the staggered grid in space-time. ρ is discretize at the beginning and end of each time interval and m is discretized on a staggered grid in space.

https://doi.org/10.4208/nmtma.2015.w02si Published online by Cambridge University Press

We discretize space-time using $n_1 \times n_2 \times n_3$ rectangular cells. For simplicity we assume uniform spacing h, yet, this can be easily generalized. Let Ω_{ijk} be the (i,j,k) box in space time. By integrating the constraint over Ω_{ijk} and using Gauss theorem along with the midpoint integration rule we obtain

$$\begin{aligned} &h^{-3}\int_{\Omega_{ijk}} \nabla^{\mathrm{st}} \cdot w \, dx\, dt = h^{-3}\int_{S_{ijk}} w \cdot n \, dS \\ =&h^{-1}\left((w_1^{i+\frac{1}{2},j,k} - w_1^{i-\frac{1}{2},j,k}) + (w_2^{i,j+\frac{1}{2},k} - w_2^{i,j-\frac{1}{2},k}) + (w_3^{i,j,k+\frac{1}{2}} - w_3^{i,j,k-\frac{1}{2}}) \right) + \mathcal{O}(h^2). \end{aligned}$$

This suggests a staggered grid discretization for the variables m_1, m_2 and ρ. Indeed, it is well known that a natural compact discretization of the divergence is staggered for both fluid dynamics, mixed formulation of the Poisson equation and Maxwell's equations [1,30]. Thus, we discretize m_1 at points $(i+\frac{1}{2},j,k)$, m_2 at $(i,j+\frac{1}{2},k)$ and ρ at $(i,j,k+\frac{1}{2})$ with $i,j,k = 0,\cdots n$. It is important to note that if non-staggered grid is used for the discretization of the divergence, instabilities arise due to null spaces of the resulting system [30]. Also, note that just like the continuous constraint, this discretization does not requires boundary conditions for m or ρ, that is a natural property for the problem at hand.

Finally, discretizing μ_0 and μ_1 and defining the vector

$$q = h^{-1}\left(\mu_0^\top, \underbrace{0,\cdots,0}_{n_1 n_2 (n_3-1)}, \mu_1^\top\right)^\top$$

we obtain a compact discretization of the constraint

$$D_1 m_1 + D_2 m_2 + D_3 \rho = q, \tag{3.1}$$

where D_j are derivative matrices in x, y and t directions.

In order to discretize the objective function we use a combination of a midpoint and a trapezoidal methods. It is straightforward to verify that for sufficiently smooth m and ρ we have

$$\begin{aligned} \int_{\Omega_{ijk}} \frac{|m|^2}{\rho}\, dx\, dt = &h^3 \frac{(m_1^{i+\frac{1}{2},j,k})^2 + (m_1^{i-\frac{1}{2},j,k})^2 + (m_2^{i,j+\frac{1}{2},k})^2 + (m_2^{i,j-\frac{1}{2},k})^2}{4\rho^{i,j,k-\frac{1}{2}}} \\ &+ h^3 \frac{(m_1^{i+\frac{1}{2},j,k})^2 + (m_1^{i-\frac{1}{2},j,k})^2 + (m_2^{i,j+\frac{1}{2},k})^2 + (m_2^{i,j-\frac{1}{2},k})^2}{4\rho^{i,j,k+\frac{1}{2}}} + \mathcal{O}(h^2). \end{aligned} \tag{3.2}$$

Abusing notations we can write the objective in matrix form as

$$\int_\Omega \frac{|m|^2}{\rho}\, dx\, dt = h^3 \left\{ \frac{A_1(m_1)^2 + A_2(m_2)^2}{A_3^+ \rho} + \frac{A_1(m_1)^2 + A_2(m_2)^2}{A_3^- \rho} \right\} + \mathcal{O}(h^2), \tag{3.3}$$

https://doi.org/10.4208/nmtma.2015.w02si Published online by Cambridge University Press

where A_1, A_2 are averaging matrices for the x and y directions and $A_3^{\pm}$ picks the appropriate ρ on each side of the space-time cube. In our notation, the expressions m^2 and $1/\rho$ is applied pointwise. This expression can also be written as

$$\int_\Omega \frac{|m|^2}{\rho}\,dx\,dt = h^3(A_s m^2)A_t\Big(\frac{1}{\rho}\Big) + \mathcal{O}(h^2), \tag{3.4}$$

where $A_s = [A_1, A_2]$ and A_t are averaging matrices in space and time with respect to vectors $m = [m_1, m_2]$ and ρ.

Note that since we use a staggered grid, averaging is needed to evaluate the objective function, which is defined pointwise. Averaging can introduce instabilities into the discretization if not done appropriately. Here we *first square then average* and *first divide then average*. These are crucial points in obtaining stable discretization (see a discussion in [1]). For example, this guarantees that $f(m,\rho) \to \infty$ as $\rho \to 0$. This property is important if we want to avoid obtaining non-physical negative densities.

4. Optimization

In this section we shortly describe the constrained optimization framework for the discrete problem

$$\begin{aligned} \min \quad & f(m,\rho) = h^3(A_s m^2)A_t\left(\frac{1}{\rho}\right) \\ \text{s.t.} \quad & C(m,\rho) := D\left[m^\top;\rho^\top\right]^\top - q = 0. \end{aligned}$$

We will use a Newton-type scheme for the solution of this constrained optimization problem. Such method bears the advantage of being mesh independent [32], that is, the number of iteration needed for convergence are independent of the mesh size. When such a method is combined with an appropriate multigrid solver for the linear system one can obtain linear complexity convergence.

Since we consider large-scale 3D and 4D space-time problems, inexact Newton solvers are inevitable. In particular, we will consider the sequential quadratic programming (SQP) method for the solution of the problem, with inexact step computation of the linearized system. We can write the Lagrangian of the problem

$$\mathcal{L}(m,\rho) = (A_s m^2)A_t\left(\frac{1}{\rho}\right) + \lambda^\top\Big(D\left[m^\top;\rho^\top\right]^\top - q\Big),$$

where λ is a Lagrange multipliers vector. From here it follows that the first order necessary conditions are

$$\nabla_m\mathcal{L} = 2MA_s^\top A_t\left(\frac{1}{\rho}\right) + (D_1, D_2)^\top\lambda = 0, \tag{4.1a}$$

$$\nabla_\rho\mathcal{L} = -RA_t^\top A_s(m^2) + D_3^\top\lambda = 0, \tag{4.1b}$$

$$\nabla_\lambda\mathcal{L} = D\left[m^\top;\rho^\top\right]^\top - q = 0, \tag{4.1c}$$

https://doi.org/10.4208/nmtma.2015.w02si Published online by Cambridge University Press

where $M := \text{diag}(m)$, $R := \text{diag}(\frac{1}{\rho^2})$.

This non-linear system of equations for m, ρ and λ can be solved in principle by using Newton's method. However, since the mixed second derivative of the objective function introduces non-diagonal terms in the Hessian, a Gauss-Newton approximation to the Hessian of the constraint is therefore sought [18].

The saddle point system which is solved inexactly at each SQP iteration can be written as

$$\begin{pmatrix} \hat{A} & D^\top \\ D & 0 \end{pmatrix} \begin{pmatrix} \delta w \\ \delta \lambda \end{pmatrix} = - \begin{pmatrix} \nabla_w \mathcal{L} \\ \nabla_\lambda \mathcal{L} \end{pmatrix}, \tag{4.2}$$

where $\hat{A} := \widehat{\nabla^2 \mathcal{L}}$ is symmetric positive definite approximation of the Hessian of the objective function

$$\hat{A} = \begin{pmatrix} 2\text{diag}(A_s^\top A_t(\frac{1}{\rho})) & 0 \\ 0 & 2\text{diag}(A_t^\top A_s(m^2)\text{diag}(\frac{1}{\rho^3}) \end{pmatrix}.$$

The saddle point system is symmetric indefinite [6]. It is also ill-conditioned, large and sparse. We will consider two solution approaches. In the first approach, we solve this system inexactly using preconditioned GMRES [29] to obtain an update for the variables

$$w \leftarrow w + \alpha \delta w, \tag{4.3}$$

$$\lambda \leftarrow \lambda + \alpha \delta \lambda, \tag{4.4}$$

where α is determined by a line search.

In order to incorporate inexactness in the solution of the linear system into the SQP framework we use a similar method to the one proposed in [10]. We base our stopping criteria for GMRES on a so-called filter [16], and will stop the linear iterations whenever the step is accepted by the filter. Thus, the GMRES solver has two stopping criteria and *both* has to be fulfilled in order to stop the iteration. First, the desired stopping criteria is achieved and second, the solution is tested by the filter. Only if both criteria are fulfilled the iteration is stopped; for further details see [16].

Since the saddle point system (4.2) is ill-conditioned, the use of suitable preconditioner is essential. We consider a preconditioner based on Schur complement (see [6] and references within)

$$\begin{pmatrix} \hat{A} & D^\top \\ 0 & S \end{pmatrix} \begin{pmatrix} \delta w \\ \delta \lambda \end{pmatrix} = - \begin{pmatrix} \nabla_w \mathcal{L} \\ \nabla_\lambda \mathcal{L} \end{pmatrix},$$

where $S = -D^\top \hat{A}^{-1} D$ is the Schur complement of the system. This preconditioner converges within three GMRES steps in exact arithmetic. The difficulty lies in inverting the Schur complement.

We should notice that since $\hat{A}$ is a diagonal matrix, its inverse can be trivially computed. Moreover, the Schur complement is a generalized Laplacian in space-time of the form $\nabla^{\text{st}} \cdot \sigma(\nabla^{\text{st}} \cdot)^*$ with coefficients $\sigma = \text{diag}(\hat{A}^{-1})$ which depends only on ρ and

https://doi.org/10.4208/nmtma.2015.w02si Published online by Cambridge University Press

m^2. Therefore, the Schur complement is suitable for multigrid methods. Since we consider models of high density contrast, we should pursue a multigrid algorithm that can account for jumping coefficient. In our algorithm we applied a single V-cycle of a Ruge-Stüben style algebraic multigrid algorithm [28] for the solution of the Schur complement part of the preconditioner.

While the above approach has optimal complexity in theory it may be slow in practice. This is due to the large setup time and memory of algebraic multigrid methods. A simpler approach that is not optimal but can converge quickly for smaller mesh is to solve the system (4.2) by elimination. We first eliminate δw, and obtain a symmetric positive definite system for $\delta\lambda$

$$-S\delta\lambda = \nabla_\lambda \mathcal{L} - D\hat{A}^{-1}\nabla_w \mathcal{L} \tag{4.5}$$

which is solved by the conjugated gradients (CG) method with a Symmetric Gauss-Seidel preconditioner. We then compute the update for w by

$$\delta w = -\hat{A}^{-1}(D^\top \delta\lambda + \nabla_w \mathcal{L})$$

and update the variables as in (4.4).

In numerical experiments we have found out that the "break even" point between the approaches is when the mesh size is roughly 64^3.

5. Numerical experiments

In our numerical experiments we would like to examine two aspects of the algorithm. Firstly, we would like to test the algorithm for the L_2 distance. Here we consider the two approaches elucidated above: a combination of GMRES and multigrid versus solution of the reduced order system by elimination and preconditioned CG. Secondly, we would like to test the behavior of the algorithm when the norm of the MK functional is gradually reduced from two to one. Note that for the L_1 norm we have that

$$f(m,\rho) = \int_\Omega \int_0^1 |m|\, dt\, dx$$

and thus the problem is not well-defined. We therefore look at the limit $p \to 1$ of

$$f(m,\rho) = \int_\Omega \int_0^1 \frac{|m|^p}{\rho^{p-1}}\, dt\, dx$$

and examine the behavior of the algorithm as we gradually reduce the norm p to one.

As a set of model problems we considered the 2D images displayed in Fig. 2. For the initial density distribution μ_0 an image of four circle quarters, one at each corner was employed. The final distribution μ_1 was represented by an image of a circle positioned in the center, where we verified that the two images have the same total volume, see Fig. 2.

https://doi.org/10.4208/nmtma.2015.w02si Published online by Cambridge University Press

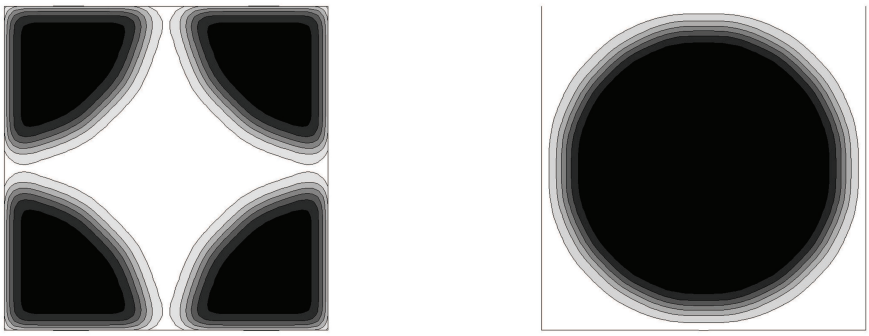


Figure 2: Left: initial density distribution image μ_0; right: final density distribution image μ_1.

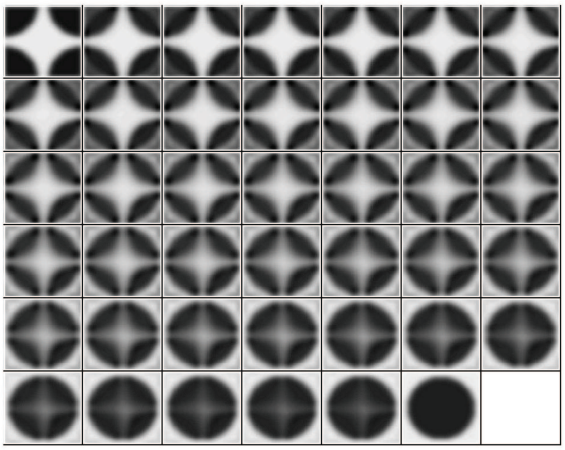


Figure 3: Solution for density distribution for $p = 2$.

For the sake of ease of computations, we considered grid size of 42×42 in space and 42 discretization steps in time, with density contrast of 10. We shall later increase the grid fineness to examine the performance of our multigrid scheme. In Fig. 3 the solution for density distributions with contrast 10 and for $p = 2$ is displayed; for each time step excluding the initial and final stage, from left to right, top to bottom.

Next we would like to check the optimality of our algorithm with respect to mesh independence behavior. The overall algorithm is optimal if its iteration count is independent with respect to the problem size, that is, if each problem is of linear complexity with respect to the number of unknowns. For this test, we considered a grid hierarchy; starting from a coarse grid of $16 \times 16 \times 10$ (in space and time) through a grids of $32 \times 32 \times 20$ to a grid of $64 \times 64 \times 40$. We set the tolerance for the outer (SQP) iteration to 10^{-4}, and as mentioned before, each step was computed inexactly up to a relative residual error tolerance of 0.1.

https://doi.org/10.4208/nmtma.2015.w02si Published online by Cambridge University Press

Table 1: Number of SQP iterations required for convergence on different grid sizes, for $p = 2$ and density contrast 10.

Grid Size	SQP iterations
$16 \times 16 \times 10$	16
$32 \times 32 \times 20$	13
$64 \times 64 \times 40$	14

Table 2: Comparison of numbers of preconditioned GMRES iterations required for convergence to the tolerance of 0.1 at 1^{st}, midst and last iteration of the SQP algorithm.

Grid Size	1^{st}	Midst	Last
$16 \times 16 \times 10$	2	3	2
$32 \times 32 \times 20$	2	5	3
$64 \times 64 \times 40$	2	6	7

In Table 1 we record the number of SQP iterations required for convergence on different grid dimensions to the desired tolerance for $p = 2$. As can be deduced from the table, the SQP algorithm is almost optimal: although the number of variables increased by a factor of 8 between the different grid sizes the number of SQP iterations required for convergence altered only mildly. In order to verify that the overall algorithm is also optimal, we need to check that the linear solver is of linear complexity. Thus, the convergence rate of the multigrid preconditioner is of particular interest. The performance of GMRES with multigrid preconditioner is presented in Table 2. In this table the inner iteration count is compared for the first iteration of SQP, an iteration in the midst of the optimization process, and the last iteration of the process. Table 2 shows a small increase in the number of iterations when the mesh is refined. Although, the number of iterations is incrementing, this increment is still negligible in comparison to the increase in mesh size. It is interesting to note that the increase in the number of iterations of the linear solver is not due to the deterioration of the multigrid solver. The reason for the increase is that the GMRES solution for a tolerance of 0.1 was determined to be inappropriate for descent by the filter. Thus more iterations in the GMRES solver where needed to fulfill the filter criteria.

In a third experiment we test our algorithm for higher density contrast. For that purpose, we consider the 2D images as before but this time with density contrast of 100. Again, our setup involve an hierarchy of models of increasing grid sizes, starting from 16×16 in space and 8 in time and up to 64×64 in space and 32 time steps. As before, we set the tolerance for the outer (SQP) iteration to 10^{-4}, and each step is computed inexactly up to a relative residual error tolerance of 0.1. In this case, we take the multi-level approach, where we interpolate the solution from the coarser grid to finer one, such that the initial guess on the finer grid is closer to the optimal solution. In Table 3 we record the number of SQP iterations required for convergence on different grid sizes to the desired tolerance for $p = 2$.

For this problem, the number of GMRES iterations was consistently two throughout the optimization process, for all grid sizes. As can be seen, the algorithm works well

https://doi.org/10.4208/nmtma.2015.w02si Published online by Cambridge University Press

Table 3: Number of SQP iterations required for convergence on different grid sizes, for $p = 2$ and density contrast 100.

Grid Size	SQP iterations
$16 \times 16 \times 8$	28
$32 \times 32 \times 16$	12
$64 \times 64 \times 32$	14

Table 4: Number of SQP iterations required for convergence on different grid sizes, for $4D$ problem, with $p = 2$ and density contrast 10.

Grid Size	SQP iterations
$16 \times 16 \times 16 \times 8$	10
$32 \times 32 \times 32 \times 16$	11
$64 \times 64 \times 64 \times 32$	10

Table 5: Comparison of numbers of preconditioned CG iterations required for convergence to a tolerance of 10^{-4} at 1^{st}, midst and last iteration of the SQP algorithm.

Grid Size	1^{st}	Midst	Last
$16 \times 16 \times 16 \times 8$	21	38	32
$32 \times 32 \times 32 \times 16$	39	86	60
$64 \times 64 \times 64 \times 32$	71	187	137

for large density contrast. No other algorithm known to us could solve this problem efficiently.

In a forth experiment, we would like to test our algorithm on 3D problems (3D in space plus time). Since we do not have an effective 4D AMG code the linear system is solved by elimination as described in Section 4. Again, we consider an hierarchy of grids, starting from $16 \times 16 \times 16$ in space and 8 time steps, through $32 \times 32 \times 32$ with 16 times step up to a grid of size $64 \times 64 \times 64$ in space and 32 time steps. In Table 4 we present the number of SQP iterations required for convergence on different grid dimension to the desired tolerance for $p = 2$. In Table 5 we summarize the number of preconditioned CG iterations required to converge to a tolerance of 10^{-4} at different stages of the SQP iterations. The table clearly demonstrates the mesh independence criteria of our algorithm even in 4D. Since we use symmetric Gauss-Seidel as a preconditioner our linear solver is not mesh independent. Nonetheless, the number of iteration grows mildly and we are still able to obtain solutions of 4D problems in a reasonable computational effort.

Finally, we test the performance of our algorithm when gradual reduction of the norm p from two to one is imposed. We shall address a 2D problem in space and time, with grid size 64×64 with 32 time steps, and density contrast 10. We elect to solve the reduced system using preconditioned CG. Simple continuation is used to obtain a solution with $p \to 1$. We start with $p = 2$ and perform a single SQP iteration. We then reduce p and repeat the process, starting from the previous solution. We use 100 continuation steps to get from $p = 2$ to $p = 1.01$. In Fig. 4 a convergence of the primal

https://doi.org/10.4208/nmtma.2015.w02si Published online by Cambridge University Press

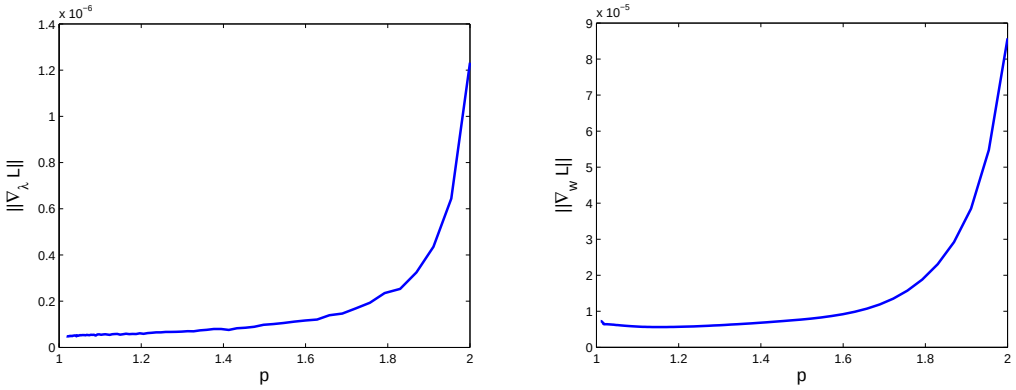


Figure 4: Left: Norm of primal feasibility as a function of norm p; right: Norm of dual feasibility as a function of norm p.

(Eq. (4.1c)) and dual feasibility (Eqs. (4.1a) and (4.1b)) are presented as a function of the norm p. As expected, the norm of primal and dual feasibility is reduced as we progress with the continuation and reduce the norm value. Although we have used a simple continuation, this was sufficient in order to obtain an approximation to the L_1 problem. More efficient continuation methods for the problem are not considered in this study.

6. Summary

A novel numerical framework for the 3D optimal mass transport problem in the fluid mechanics formulation is proposed. The new framework treats the time dependency of the PDE as another spatial dimension in staggered grid discretization. This formulation does not require boundary conditions for the density distribution explicitly. Instead, these boundary conditions are introduced implicitly as part of our optimization scheme. In order to account for large density contrast in the models, we have incorporated an algebraic multigrid as preconditioner for the solution of the linearized system. This approach proved to be optimal with respect to mesh size. We have also considered a distance function for general norm p, where $1 < p \leq 2$. We started our iterations at $p = 2$ and slowly relaxed the norm until $p = 1.01$, while performing only few iterations for each p.

From an imaging perspective, the transformation of the initial density distribution closely resembles the final distribution, which indicates a good correspondence and overall good performance of the proposed algorithm.

Acknowledgments We would like to thank Scott McCallen for the Ruge-Stüben multigrid code. EH was partially supported by NSF grants DMS 0724759, CCF-0728877 and CCF-0427094 and NSERC industrial research chair program.

https://doi.org/10.4208/nmtma.2015.w02si Published online by Cambridge University Press

References

[1] U. Ascher, *Numerical Methods for Evolutionary Differential Equations,* SIAM, Philadelphia 2008.

[2] L. Ambrosio, *Lecture Notes on Optimal Transport Theory*, CIME Series of Springer Lecture Notes, Euro Summer School Mathematical Aspects of Evolving Interfaces, Madeira, Portugal, Springer-Verlag, New York, 2000.

[3] S. Angenent, S. Haker, and A. Tannenbaum, Minimizing flows for the Monge-Kantorovich problem, *SIAM J. Math. Analysis* **35** (2003), pp. 61–97.

[4] J. Bear, Dynamics of Fluids in Porous Media, *Dover Publications, New York,* (1972).

[5] J. D. Benamou and Y. Brenier, A computational fluid mechanics solution to the Monge-Kantorovich mass transfer problem, *Numer. Math.*, **84** (2000), pp. 375–393.

[6] M. Benzi, G. H. Golub, and J. Liesen, Numerical solution of saddle point problems, *Acta Numerica*, **14** (2005), pp. 1-137.

[7] Edited by Lorenz T. Biegler, Omar Ghattas, Matthias Heinkenschloss, David Keyes, and Bart van Bloemen Waanders, Real-Time PDE-Constrained Optimization, *SIAM Philadelphia* (2007).

[8] A. Borz and K. Kunisch, A globalization strategy for the multigrid solution of elliptic optimal control problems, *Optimization Methods and Software*, **21(3)** (2006), pp. 445–459.

[9] F. Brezzi and M. Fortin, Mixed and Hybrid Finite Element Methods, *Springer-Verlag*, (1991).

[10] R. H. Byrd, F. E. Curtis, and J. Nocedal, An Inexact SQP Method for Equality Constrained Optimization, *SIAM J. on Optimization*, **19** (2008), pp. 351-369.

[11] R. Chartrand, K. Vixie, B. Wohlberg and E. Bollt, A gradient descent solution to the Monge-Kantorovich problem, submitted to *SIAM J. Sci. Comput.,* (2005).

[12] M. Cullen and R. Purser, An extended Lagrangian theory of semigeostrophic frontogenesis, *J. Atmos. Sci.*, **41** (1984), pp. 1477-1497.

[13] E. J. Dean, R. Glowinski, Numerical methods for fully nonlinear elliptic equations of the Monge-Amp‘ere type, to appear, Comput. Methods Appl. Mech (2008).

[14] G. L. Delzanno, L. Chacón, J. M. Finn, Y. Chung and G. Lapenta, An optimal robust equidistribution method for two-dimensional grid adaptation based on Monge-Kantorovich optimization, *Journal of Computational Physics archive*, **227(23)**, (2008), pp. 9841–9864.

[15] L. C. Evans, *Partial differential equations and Monge-Kantorovich mass transfer,* in *Current Developments in Mathematics,* International Press, Boston, MA, 1999, pp. 65–126.

[16] R. Fletcher, S. Leyffer and Ph. L. Toint, A Brief History of Filter Methods, *SIAG/Optimization Views-and-News*, **18** (2007).

[17] M. D. Gunzburger, Prespectives in flow control and optimization, *SIAM*, Philadelphia, 2003.

[18] E. Haber and U. Ascher and D. Oldenburg, On Optimization Techniques for Solving Nonlinear Inverse Problems, *Inverse Problems,* **16** (2000), pp. 1263–1280.

[19] E. Haber, T. Rehman, A. Tannenbaum, An Efficient Numerical Method for the Solution of the L2 Optimal Mass Transfer Problem, to appear, *SIAM J. on Scientific Computing*.

[20] E. W. Jenkins, C. T. Kelley, C. T. Miller, and C. E. Kees, An Aggregation-based Domain Decomposition Preconditioner for Groundwater Flow, *SIAM J. Sci. Comp.,* **(23)** (2001), pp. 430-441.

[21] L. V. Kantorovich, On a problem of Monge, *Uspekhi Mat. Nauk.*, **3** (1948), pp. 225–226.

[22] J. D. Moulton, J. E. Dendy, and J. M. Hyman, The black box multigrid numerical homogenization algorithm, *J. Comput. Phys.,* **141** (1998) pp. 1–29.

[23] R. A. Nicolaides, Existence, Uniqueness and Approximation for Generalized Saddle Point

https://doi.org/10.4208/nmtma.2015.w02si Published online by Cambridge University Press

Problems, *SIAM Journal on Numerical Analysis,* **18** (1982), pp. 349–357.
[24] A. Oberman, Wide stencil finite difference schemes for the elliptic Monge-Ampere equation and functions of the eigenvalues of the Hessian, *Discrete and Continuous Dynamical Systems series B (DCDS B)*, **10** (2008), pp. 221–238.
[25] V. Oliker and L. Prussner, On the numerical solution of the equation $z_{xx}^2 + z_{yy}^2 - z_{xy}^2 = f$ and its discretizations, *Numerische Mathematik*, **54** (1988), pp. 271–293.
[26] S. Rachev and L. Rüschendorf, *Mass Transportation Problems*, Vol. I, Probab. Appl., Springer-Verlag, New York, 1998.
[27] J. Rubinstein and G. Wolansky, Intensity control with a free-form lens, *J. Opt. Soc. Am. A*, **24** (2007), pp. 463–469.
[28] J. Ruge, K. Stben, Algebraic multigrid, in: S.F. McCormick (Ed.), Multigrid Methods, *Frontiers in Applied Mathematics*, **(3)**, SIAM, Philadelphia (1987), pp. 73–130.
[29] Y. Saad and M. H. Schultz, GMRES: a generalized minimal residual algorithm for solving nonsymmetric linear systems, *SIAM J. Sci. Stat. Comput.*, **7** (1986), pp. 856-869.
[30] U. Trottenberg, C. Oosterlee and A. Schulle, *Multigrid*, Academic Press, 2001.
[31] C. Villani, *Topics in Optimal Transportation,* Graduate Studies in Mathematics, vol. 58, AMS, Providence, RI, 2003.
[32] S. Volkwein, Mesh-Independence of Lagrange-SQP Methods with Lipschitz-Continuous Lagrange Multiplier Updates, *Optimization Methods and Software*, **17** (2002), pp. 77-111.

https://doi.org/10.4208/nmtma.2015.w02si Published online by Cambridge University Press